IEICE TRANS. FUNDAMENTALS, VOL.E102–A, NO.12 DECEMBER 2019

PAPER Special Section on Smart Multimedia & Communication Systems

Frequency Efficient Subcarrier Spacing in Multicarrier Backscatter Sensors System

Jin MITSUGI[†a)], **Yuki SATO**[†], **Yuusuke KAWAKITA**[††], *and* **Haruhisa ICHIKAWA**[†††], *Members*

SUMMARY Backscatter wireless communications offer advantages such as batteryless operations, small form factor, and radio regulatory exemption sensors. The major challenge ahead of backscatter wireless communications is synchronized multicarrier data collection, which can be realized by rejecting mutual harmonics among backscatters. This paper analyzes the mutual interferences of digitally modulated multicarrier backscatter to find interferences from higher frequency subcarriers to lower frequency subcarriers, which do not take place in analog modulated multicarrier backscatters, is harmful for densely populated subcarriers. This reverse interference distorts the harmonics replica, deteriorating the performance of the existing method, which rejects mutual interference among subcarriers by 5 dB processing gain. To solve this problem, this paper analyzes the relationship between subcarrier spacing and reverse interference, and reveals that an alternate channel spacing, with channel separation twice the bandwidth of a subcarrier, can provide reasonably dense subcarrier allocation and can alleviate reverse interference. The idea is examined with prototype sensors in a wired experiment and in an indoor propagation experiment. The results reveal that with alternate channel spacing, the reverse interference practically becomes negligible, and the existing interference rejection method achieves the original processing gain of 5 dB with one hundredth packet error rate reduction.

key words: *backscatter communications, interference rejection, software defined radio, harmonics*

1. Introduction

1.1 Background

Wireless sensors are expected to lower the installation cost, and to increase the sensor density of automated structural health monitoring (SHM) [1], [2]. The apparent problem of battery-powered wireless sensors is the necessity to replace the power source (battery) from time to time. Replacements of battery incur human interventions, which are major sources of errors, and prevent sensors from being implanted into artifacts. To counter this problem, batteryless wireless sensors are of immense research interests [3]. However, even a batteryless sensor needs to harvest power to establish a two-way communication link.

Backscatter communications [4], [5], which is extensively used in RFID, can achieve batteryless sensing and establish a two-way communication link. In a backscatter communication system, a dedicated reader generates powering radio wave and transmits it to a group of wireless sensors. The principle of a backscatter communications system is illustrated in Fig. 1. The powering wave is either modulated to provide commands from the reader to the sensors (hereinafter forward link) or continuous wave (CW), which supplies power to the sensors. The return link (sensor to reader) can be produced by changing the impedance of the wireless sensor antenna – typically the matched state and the short circuit (total reflection) – with an embedded RF switch. An analog modulated backscatter can be produced by embedding an analog modulator in the sensor, with which the sensor data modulates CW [6], [7]. [6] used electret condensor microphone (ECM) and a junction gate field-effect transistor (JFET) to produce amplitude-modulated backscatter. [7] used a commercial phase shifter (Skyworks PS088-315) to produce phase-modulated backscatter. Sensor data can alternatively be acquired by the logic circuit with an AD converter or a digital interface, such as serial peripheral interface (SPI), and by digitally modulating CW. When digital modulation is employed, the modulator block in Fig. 1 is not needed.

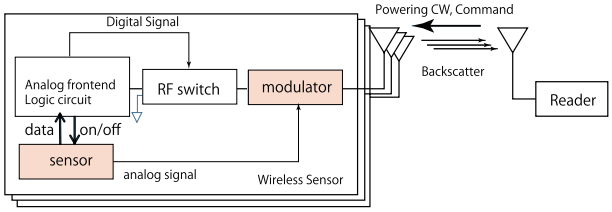

Fig. 1 Backscatter wireless sensor can send sensing signal by changing the antenna impedance.

A backscatter communications system can eliminate the need for batteries, power amplifiers and synthesizers in sensors, which reduce the complexity of sensor, resulting in the low cost and small form factor, typically an LSI size. Backscatter communication sensors are exempt from radio regulations, and can be flexibly used across countries by using a reader that conforms to regulations.

To separate the inherently weak return link from the phase noise of the powering or neighbor forward link, a constant rate RF switching at the sensor is applied to the baseband signal to shift the backscatter signal away from the CW in frequency domain. This is referred to as a subcarrier [8] and is extensively used in industrial RFID deployment owing to its robustness against the interferences from neighbor

Manuscript received February 14, 2019.
Manuscript revised June 11, 2019.

[†]The authors are with Keio University, Fujisawa-shi, 252-0882 Japan.
[††]The author is with Kanagawa Institute of Technology, Atsugi-shi, 243-0292 Japan.
[†††]The author is with The University of Electro-Communications, Chofu-shi, 182-8585 Japan.
a) E-mail: mitsugi@keio.jp

DOI: 10.1587/transfun.E102.A.1834

systems [9]. Backscatter can be produced by reflecting not only dedicated CW but also ambient radio power [10], [11].

According to Noel [12], when wireless sensors, not restricted to backscatter sensors, are applied to automated SHM, they shall meet the following requirements.

1. Sensor sampling rate ranges from 100 Hz to 1,000 Hz.
2. The number of sensors is up to 70.
3. Sensor data synchronization is below 120 μs.

The requirements on the number of sensors and their synchronization are important to accurately measure the instantaneous structural response against an exciting force. Therefore, meeting the two requirements is the primary challenge of wireless sensors for SHM applications, particularly of batteryless wireless sensors. This paper aims to fulfill the requirements in a frequency efficient manner by rejecting harmonics among backscatters with artificially produced replicas, and by securing appropriate channel separation among backscatters.

1.2 Related Works

Fu et al. [13] present simultaneous imaging and localization with orthogonal spread spectrum codes in the preamble of a backscatter frame. They confirmed the performance of the proposal with two time-synchronized sensors. Such spread spectrum multiple access (SSMA) or code division multiple access (CDMA) approach can be found in other literature such as [14], [15]. However, the approach suffers from the unavoidable near-far problems because of the absence of the transmission power control of the backscatter and the loss of backscatter orthogonality due to the unstable, and thus inevitably unsynchronized, clocks in backscatter sensors.

Hu et al. [16] proposed Laissez-Faire where the envelope of multiple backscatters are analyzed and separated at the reader. They successfully separated up to 16 simultaneous streams in experiments. This method demands clear envelope of backscatter, which are only available in high carrier to interference ratio (CIR) environments. In practical propagation environments, however, envelope are usually unclear in low CIR conditions. Because of this waveshape distortion in low CIR environments, Laissez-Faire will work only in high CIR environments.

Simultaneous use of multiple subcarriers was proposed by Vannuci et al. [17] in which the sensor uses a minimum shift keying (MSK) subcarrier to reduce the harmonics, and uses a narrowband signal (low bitrate). The authors of [17], however, did not introduce any interference canceler, because they assumed that the possible communication outage having resulted from the interferences were ignored. Because the low outage rate is attributed to the low density subcarrier allocation (10 bps bandwidth for up to 200 kHz subcarrier), the method suffers from the wide bandwidth requirements for a large number of backscatter sensors.

Reduction of the direct current (DC) component with a set of codewords has been extensively studied in the field of storage systems [18]. Disparity, which is the difference between the numbers of marks and spaces, can be zero or low while the code rate is nearly equal to one, when using long codewords. However, such a DC-balanced code demands a long state-machine or a large codebook for wireless sensors. There are interesting studies on perfect pulses [19], [20] to suppress harmonics by enforcing smooth transitions with higher clock rates in sensors, in a manner similar to MSK.

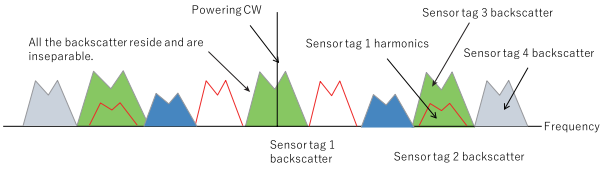

Fig. 2 Pseudo FDMA can be realized by using multiple subcarriers concurrently. But we need to reject unavoidable harmonics.

1.3 Our Approach and the Problem Statement

In parallel to these existing studies, the authors of this paper propose a multiple access method that uses multiple subcarriers concurrently to establish pseudo frequency division multiple access (FDMA) in backscatter communications [21], [22]. The reason we refer to the method as "pseudo" is because a backscattered subcarrier inevitably generates harmonics. Harmonics interfere with other channels as shown in Fig. 2. By mathematically producing replicas of subcarrier harmonics and subtracting them from the observed signal, individual baseband signals that are superposed onto subcarriers can be extracted. We refer to this method as multiple subcarrier multiple access (MSMA). The salient feature of MSMA is the harmonics rejection method, referred to as MSMA interference rejection in this paper, which exploits the harmonics characteristics of being generated only in higher subcarrier channels.

While Miller coding, a standard short zero disparity code [8], is used in the evaluations in this work, MSMA interference rejection can work with other zero or low disparity codes. We may alternatively avoid the harmonics of subcarriers interfering with other subcarrriers by placing subcarriers away from the CW. However, in such placement, the sensor's clock rate needs to be increased, resulting in larger power consumption. We also need to be careful not to expose the subcarriers to other radio systems that are authorized to use the same frequency band.

As introduced in past [7], [22], we confirmed the fundamental principle of MSMA works for analog (phase or frequency) modulated subcarriers. Analog modulated MSMA suffers from unavoidable phase fluctuation caused by, for example, the movement of target artifact or humans in practical environments. This instability confines the use of analog modulated MSMA only in propagation controlled environments such as in an anechoic chamber. Because MSMA rejects harmonics before the demodulation, it also works on digitally modulated subcarriers. In [23], we applied a digital modulation in MSMA to reveal its practical-

ity in an out-door radio propagation environment with four backscatter sensors. During the course of this development, we noticed that the interference rejection method did not work well at times.

As we explain later in this paper, the harmonics of a digitally modulated subcarrier interfere not only with the higher frequency subcarriers but also the lower frequency subcarriers. We refer to this problem as "reverse interference" in this work. The accommodation of the reverse interference into the mathematical formulation of interference rejection is possible, albeit complex. In this paper, the reverse interference problem is solved by securing sufficient separation between subcarriers, instead of producing the rigorous harmonic replicas.

The rest of this paper is organized as follows. Although the principle of harmonics rejection in MSMA was proposed in [22], Sect. 2 explains the signal model in backscatter communications tailoring to the digital modulation for completeness. The reverse interference problem associated with digital modulation is also introduced in Sect. 2. This section clarifies that sufficient subcarrier separation suppresses reverse interference in practice. In Sect. 3, the fundamental performance of interference rejection in a wired and a wireless configuration experiments, where the replicas of harmonics may be distorted by reverse interference, are reported. Section 4 concludes the paper.

2. Digitally Modulated Multiple Subcarrier Multiple Access Theory

In this section, we first explain the subcarrier backscatter signal model with digital modulation. The fundamental difference between digitally modulated and analog modulated subcarriers is the infinite bandwidth caused by the phase discontinuity in a digitally modulated subcarrier. We later show that this problem can be practically solved by securing sufficient spacings among subcarriers.

2.1 Subcarrier Backscatter Signal Model

A subcarrier backscatter is produced by a constant rate on/off keying of antenna impedance of a sensor. Figure 3 shows the general backscatter signal at the reader receiver ingress where the time is normalized with the subcarrier period, T_s, and m denotes the modulation index. Because the clock timing of a sensor usually differs from that of the corresponding reader, we introduce a phase delay of subcarrier as ϕ_d. The phase delay is combined with the digital phase component ϕ_i depending on the baseband signal encoding, such as Miller and FM0, either $i = 0$ or $i = 1$, typically $\phi_0 = 0$ and $\phi_1 = \pi$ are used. The total phase is therefore $\phi = \phi_d + \phi_i$. Because the carrier phase at a sensor depends on the distance between the reader and the sensor, and the modulated phase, the reverted carrier is assumed to have a Ψ phase delay at reader. Denoting the carrier angular velocities as ω_c, the modulated subcarrier signal $S(t)$ at the reader receiver ingress can be written as

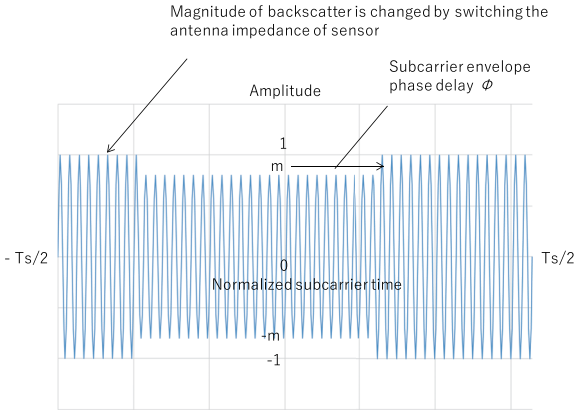

Fig. 3 Backscatter subcarrier waveform at the reader receiver. The envelop is changed by a constant rate toggling of an RF switch.

$$S(t) = s_e(t)\boldsymbol{e}^{j(\omega_c t+\Psi)}, \tag{1}$$

where $s_e(t)$ denotes the square waveform envelope after the attenuation due to propagation.

The frequency components of the square waveform envelope, $s_e(t)$, can be derived by applying Fourier series based on the subcarrier angular velocity, ω_s as follows.

$$s_e(t) = m + 1 + \alpha \sum_{n=1,3,\cdots} \frac{1}{n} \sin(n\omega_s t - n\phi), \tag{2}$$

where

$$\alpha = \frac{2(1-m)}{\pi}.$$

Equation (2) shows that the higher harmonics accompany longer phase delay. This is well-known linear group delay. It is also shown in Eq. (2) that the harmonics of a subcarrier appear only in odd multiples of the primary subcarrier channel, and the amplitude of higher harmonic decays with the reciprocal of n.

Substituting Eq. (2) into Eq. (1), the received signal can be rewritten as follows.

$$\begin{aligned} S(t) &= (m+1)\boldsymbol{e}^{j(\omega_c t+\Psi)} \\ &\quad + \alpha \sum_{n=1,3,\cdots} \frac{1}{n} \sin(n\omega_s t - n\phi)\boldsymbol{e}^{j(\omega_c t+\Psi)} \end{aligned} \tag{3}$$

The receiver down-converts the incoming subcarrier signal, $S(t)$, by multiplying the carrier signal $\boldsymbol{e}^{-j\omega_c t}$ and applies a high pass filter (HPF) to achieve the maximum resolution of backscatter to yield the baseband signal $S_b(t)$ such that

$$\begin{aligned} S_b(t) &= \alpha \sum_{n=1,3,\cdots} \frac{1}{n} \sin(n\omega_s t - n\phi)\boldsymbol{e}^{j(\omega_c t+\Psi)}\boldsymbol{e}^{-j\omega_c t} \\ &= \alpha \sum_{n=1,3,\cdots} \frac{1}{n} \sin(n\omega_s t - n\phi)\boldsymbol{e}^{j\Psi}. \end{aligned} \tag{4}$$

Because ϕ comprises the phase delay and the modulation phase such that $\phi = \phi_d + \phi_i$, Eq. (4) can be rewritten as

$$S_b(t) = \alpha \sum_{n=1,3,\cdots} \frac{1}{n} \sin(n\omega_s t - n\phi_d - \phi_i) e^{j\Psi}, \quad (5)$$

where the relationship, $n\phi_i = \phi_i$ holds because any odd number n can be expressed as $n = 2m + 1$ and $\phi_i = 0$ or π, yielding $n\phi_i = \phi_i + 2m\phi_i = \phi_i$. Equation (5) indicates that the same bandwidth appears at every harmonic component.

The IQ components after the down-conversion are obtained as follows.

$$I = \alpha \sum_{n=1,3,\cdots} \frac{1}{n} \sin(n\omega_s t - n\phi_d - \phi_i) \cos\Psi$$
$$Q = \alpha \sum_{n=1,3,\cdots} \frac{1}{n} \sin(n\omega_s t - n\phi_d - \phi_i) \sin\Psi \quad (6)$$

In this set of equations, $n = 1$ represents the primary subcarrier. Components $n > 1$ are the harmonics. Each of the frequency component can be extracted by applying a band pass filter (BPF). Because either I or Q component only comprises a sine wave, S_b produces a straight line in the IQ plane. This characteristic is known as a zero-cross signal [24].

The phase discontinuity in digital modulation produces infinitesimal harmonics in the modulated signal, which decay with frequency separation. A continuous phase frequency shift keying (CPFSK), typically MSK can reduce the harmonics, as proposed in [17]. However, in this case, the frequency deviation of the harmonics becomes wider than that of the primary subcarrier because the convenient characteristic $n\phi_i = \phi_i$ is no longer valid. The caveat to employing digital modulation in MSMA is, therefore, to avoid any possible adjacent channel interference, particularly the reverse interference, which is not observed in analog modulation.

2.2 Digitally Modulated Signal

The raw bit rate of digitally modulated subcarrier – assuming that no coding is applied – is determined by dividing the subcarrier frequency by the number of subcarrier cycles m_s to represent one bit. The waveform of a single-bit signal for several m_s is shown in Fig. 4. Supposing that those waveforms in Fig. 4 represent marks (1 s) then their phase-reversed signals represent spaces (0 s) in BPSK. Note that for all the m_s cases, the bit rates and the required bandwidth remain unchanged because the one-bit duration is constant.

The adjacent channel interference of three subcarriers is calculated as shown in Fig. 5 by applying Fourier series to the waveforms in Fig. 4. It is assumed that any subcarrier has the same power at the receiver. The channel power in Fig. 5 is, therefore, normalized with the peak power. As is seen in Fig. 5, the main interference source to subcarrier 3 is the harmonic of subcarrier 1. The adjacent leakage from channel 2 is about 8 dB less than the harmonic.

Because $m_s = 2$ produces the most densely populated subcarriers frequency-wise, the adjacent channel interference, including reverse interference, is large. The reverse

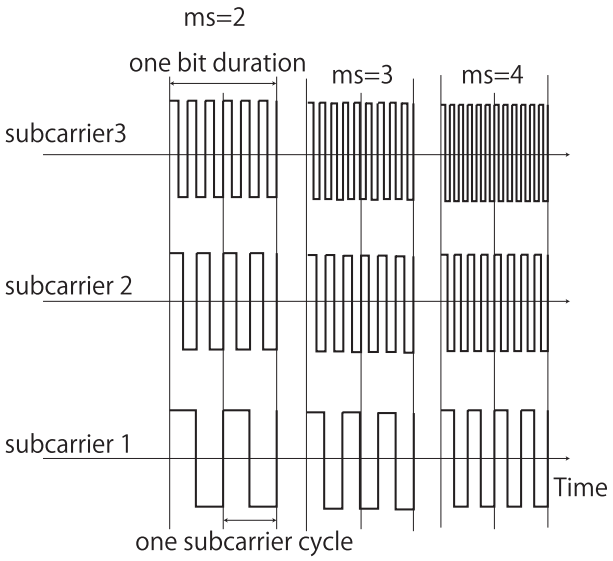

Fig. 4 Time domain signal of single bit subcarrier.

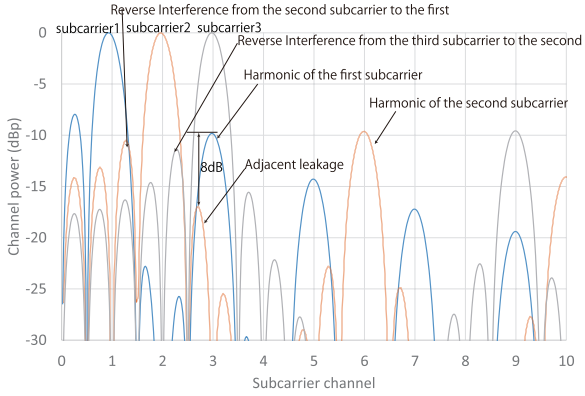

Fig. 5 Adjacent channel interference among subcarriers in case $m_s = 2$.

interference on the first subcarrier is particularly severe because the negative frequency components of harmonics of digitally modulated signals are reflected at the carrier frequency, and they spill over to the positive frequency domain.

For comparison, the spectrum in the case of $m_s = 4$ is shown in Fig. 6. By comparing Figs. 5 and 6 it is clear that the adjacent channel interference can be mitigated by securing wider subcarrier channel separation.

The aggregated reverse interference on the first subcarrier from the second and third subcarriers are calculated as in Fig. 7 assuming that after the fourth subcarrier the reverse interference on the first subcarrier is negligibly small. In the case of $m_s = 4$, the CIR of the first subcarrier is approximately 14 dB. The CIR is calculated by dividing the subcarrier 1 channel power (0 dB) by the aggregated reverse interference from subcarriers 2 and 3, which is sufficiently high for BPSK demodulation. With these observations, it is shown that digitally modulated MSMA is feasible when sufficient subcarrier spacing is secured by using more than three subcarrier cycles to represent a bit. However, the increase of subcarrier spacing deteriorates frequency effi-

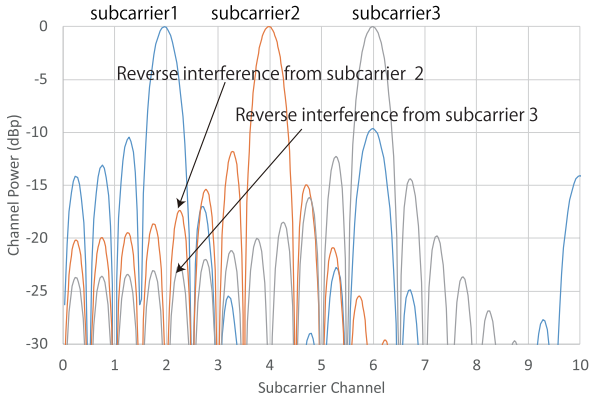

Fig. 6 Adjacent channel interference among subcarriers in case $m_s = 4$.

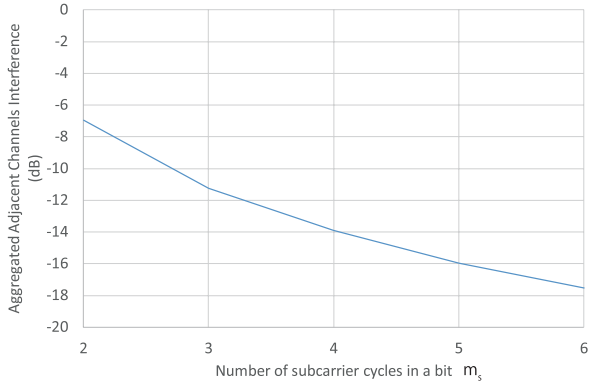

Fig. 7 Aggregated adjacent channel interference on the first subcarrier.

ciency. From Fig. 7, a reasonable tradeoff is observed to be $m_s = 4$, because the improvement in CIR somewhat saturates for $m_s > 4$.

3. Performance Evaluation of Digitally Modulated MSMA

3.1 Prototype System

We developed a prototype MSMA system using USRP 2952R and LabVIEW Communications as the transmitter and the receiver. The host PC on which LabVIEW communications runs is equipped with Win7 Core i7, 4.0 GHz clock, with a memory of 64 GB.

The prototype backscatter sensor uses a CPLD (Intel MAX V) and an MCU (Atmel SAML21) as shown in Fig. 8. We did not implement a crystal oscillator in the prototype sensor, but used the internally generated clock of the MCU to emulate the low-stability clock of LSI sensor. A clock rate of 4 MHz was used in the experiment. The prototype sensor was housed in a water-proof case for outdoor experiments.

The subcarrier frequencies and subcarrier channel separation m_s of the prototype sensor can be changed by using an embedded DIP switch and also by changing the firmware. The sensor modulates its subcarrier with a predefined pattern or a 12 bit A/D converted external analog signal. In

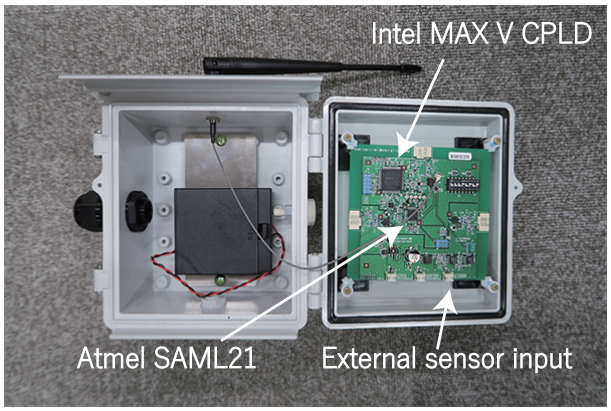

Fig. 8 Prototype backscatter sensor.

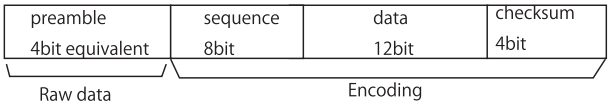

Fig. 9 Packet structure of digitally modulated streaming.

either case, 8 bit sequence number, data and 4 bit check sum are Miller encoded, and adding 4 bit equivalent preamble which violates the Miller encoding to facilitate the frame synchronization as shown in Fig. 9. Each sensor continuously modulates the subcarrier with the sequence of packets.

3.2 Subcarrier Separation and MSMA Interference Rejection

We use three sensors – sensor 1, sensor 2 and sensor 3 – which are allocated with three consecutive subcarrier channels, $f_s, 2f_s, 3f_s$ where f_s is the unit subcarrier frequency of sensor1. Because of the principle of subcarrier harmonics, sensor 1 always interferes with sensor 3 channel. If there is a harmful reverse interference from sensor 2 on sensor 1, the replica of sensor 1 harmonic in the sensor 3 channel gets distorted. As a result, the performance of MSMA interference rejection for the sensor 3 channel deteriorates. Those sensors are connected to a USRP2952R with SMA cables and an attenuator to adjust CIR. Because the bit-rate is 10 kbps in any case and any sensor, the channel separations in $m_s = 2$, $m_s = 3$, $m_s = 4$ are equivalent to one, one and half and twice the bandwidth defined in Fig. 4, respectively. We use $f_s = 20$ kHz, 30 kHz, 40 kHz, and 50 kHz to represent $m_s = 2, 3, 4, 5$ settings, respectively, as shown in Table 1. Because the master clock of sensor is 4 MHz, there may be a frequency difference between sensor 3 and the harmonic of sensor 1. The calculated frequency differences are denoted by the Δf column in the table. It is shown that the frequency difference is within the one-side bandwidth of 5 kHz. The experimental setup is shown in Fig. 10.

In each set of parameters, we collected at least 10,000 packets from sensor 3, which is subjected to the interference from sensor 1, and calculated the packet error rate. The result is shown in Fig. 11. In the figure, the broken lines

Table 1 Subcarrier allocation in each m_s setting.

m_s	f_s	$2f_s$	$3f_s$	Δf (kHz)
2	20	40	60	0.6
3	30	60	90	0.7
4	40	80	120	1.2
5	50	100	150	3.8

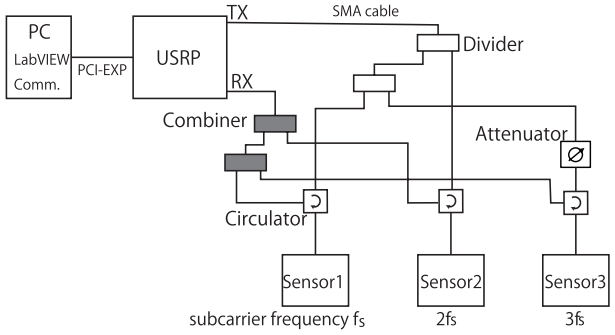

Fig. 10 Experimental setup to evaluate the contribution of subcarrier separation.

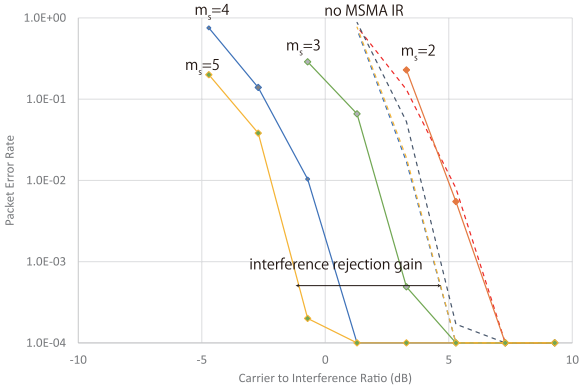

Fig. 11 Contribution of subcarrier spacing on the interference rejection.

marked "no MSMA IR" denote the group of packet error ratios of $m_s = 2, 3, 4$ and 5 without MSMA interference rejection. The lines with markers are the packet error rates with MSMA interference rejection.

The packet error rates without MSMA interference rejection are clustered in Fig. 11, and are invariant to the number of subcarrier spacings. MSMA interference rejection does not function well under a dense subcarrier allocation (typically $m_s = 2$). This is because of the reverse interference from sensors 2 and 3 to the sensor 1 channel as shown in Fig. 7 distorts the harmonics replica. When the subcarrier spacing is increased to $m_s = 3$ or 4 the interference rejection performance improves. When the alternate channel allocation, $m_s = 4$, is used, interference rejection processing gain of approximately 5 dB is achieved. The packet error rate is improved by approximately one hundredth at CIR = 5 dB. If the subcarrier spacing is further increased to $m_s = 5$ some improvements in the low CIR environment are observed. However, in the high CIR environment, the contribution of channel separation is saturated. This result

Table 2 5 kHz subcarrier allocation patterns.

Pattern	sensor 1	sensor 2	sensor 3	Δf (kHz)
A	35	45	105	0.0
B	40	50	120	1.2
C	45	55	135	1.6
D	50	60	150	3.8

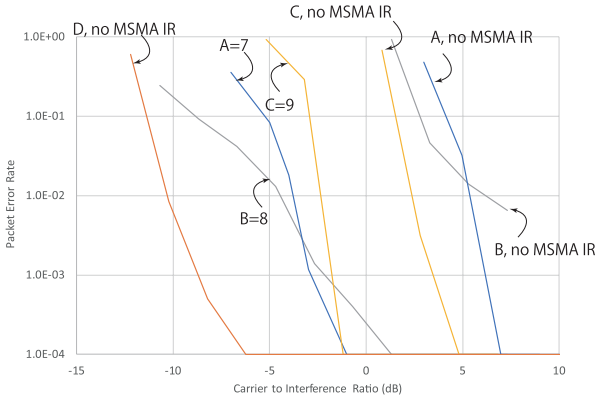

Fig. 12 Contribution of subcarrier spacing on the interference rejection when the bandwidth of each subcarrier is 5 kHz.

agrees with our expectations laid in Sect. 2.2.

To confirm the consistent effectiveness of alternate subcarrier spacing in different bandwidth signals, another experiment using narrow signal of 5 kbps was conducted with three sensors with and without MSMA interference rejection. In this experiment, the subcarrier separation between sensors 1 and 2 was always 10 kHz, double of the bandwidth, and sensor 1 always interferes sensor 3 as shown in Table 2. Note that the frequency difference in pattern D, 3.8 kHz, exceeds the bandwidth, 2.5 kHz. The packet error rate of sensor 3 was measured by collecting at least 10,000 packets. The results are shown in Fig. 12.

The packet error rates without MSMA interference rejection are equivalent to those of 10 kbps bandwidth cases in Fig. 11. The packet error rate of pattern D without MSMA interference was better than those of other cases with MSMA interference rejection. This is because the frequency difference, 3.8 kHz, exceeds the one-side bandwidth of 2.5 kHz, resulting in no harmful interference to the bandwidth of sensor 3. The processing gains of patterns A, B and C are equivalent to those of the 10 kHz bandwidth cases shown in Fig. 11.

3.3 Digital MSMA in an Indoor Wireless Environment

To evaluate the performance of MSMA interference rejection subjected to wireless propagation, we conducted an indoor wireless communications experiment with five prototype sensors $1 \sim 5$, as shown in Figs. 13 and 14. We used two circular polarized antennas in a bi-static configuration – separated transmitting and receiving antennas. The gain of the antennas are 6 dBi. The transmission power is 23 dBm. The distance between the reader and the prototype sensors is about 2 m. In the experiment, sensors $1 \sim 5$ use 20 kHz,

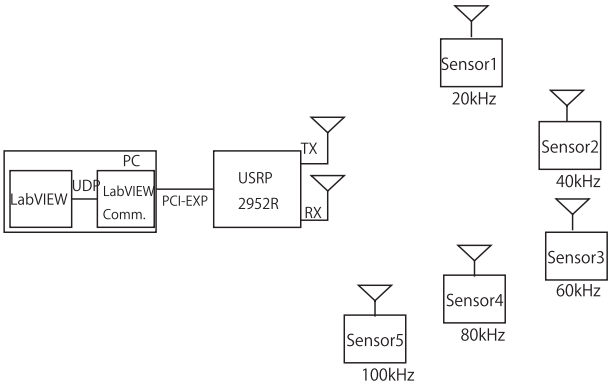

Fig. 13 Digital MSMA indoor experiment schematics.

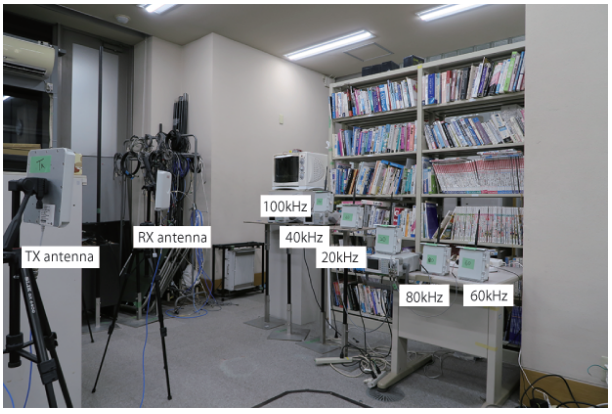

Fig. 14 The indoor experiment was conducted in our laboratory.

40 kHz, 60 kHz, 80 kHz and 100 kHz subcarriers, respectively with $m_s = 4$ and 10 kHz bandwidth each. Predefined signal patterns, generated by the MCU in each sensor, were used as sensor data in this experiment.

In this arrangement, the first and second harmonics of sensor 1 interfere with sensor 3 and sensor 5 channels, respectively. The packet structure is the same as that in Fig. 9. CIR in the channels of sensor 3 and 5 were estimated by measuring the harmonics power by switching off sensor 3 or 5, and signal power by switching off sensor 1. The positions of the five sensors were changed six times to yield different CIR patterns. We collected at least 10,000 packets from each sensor to calculate packet error rate.

The packet error rates of sensors 3 and 5 with and without MSMA interference rejection are shown in Fig. 15, in which the measurements with and without MSMA interference are represented by triangular and circular markers. The packet error rates in the wired experiment (Fig. 11, $m_s = 4$) are overwritten by solid lines for comparison.

Although the measured packet error rate characteristics for both with and without MSMA interference are degraded by several decibels from those of the wired experiment results, the contribution of interference rejection is clearly shown in the result. At CIR = 5 dB, the packet error rate improvement with MSMA interference rejection exceeds one hundredth, which is equivalent to the wired experiment result in Fig. 11. The result shows that the alternate subcarrier subcarrier spacing works in real world propagation environment.

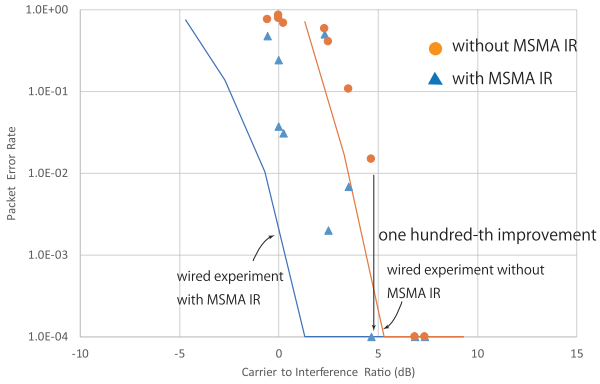

Fig. 15 MSMA interference rejection performance in the indoor experiment.

4. Conclusion

Because of the harmonics produced by the digitally modulated subcarrier, digital MSMA may involve reverse interference — interferences from high subcarrier frequency sensors to low subcarrier frequency sensors. The reverse interference deteriorates the convenient spectral characteristics among the interfering and interfered sensors. Straightforward implementation of the interference rejection algorithm using harmonics replicas may not work in digitally modulated MSMA as in the case of analog modulation. The problem can be solved by properly securing subcarrier spacing; specifically, in the alternate arrangement. The frequency-efficient spacing can alleviate reverse interference, and can still allow a fairly dense subcarrier allocation, while preserving the original processing gain of approximately 5 dB with one hundredth packet error rate improvement.

Acknowledgments

This research and development work was supported by the MIC/SCOPE #185003004.

References

[1] K. Smarsly, K. Dragos, and J. Wiggenbrock, "Machine learning techniques for structural health monitoring," 8th European Workshop on Structural Health Monitoring, pp.1–10, 2016.
[2] H. Sohn, C. Farrar, F. Hemez, D. Shunk, D.W. Stinemates, B.R. Nadler, and J.J. Czarnecki, "A review on structural health monitoring literature: 1996-200," Technical Report, Los Alamos National Laboratory, 2004.
[3] A. Deivasigamani, A. Dalirim, C.H. Wang, and S. John, "A review of passive wireless sensors for structural health monitoring," Modern Applied Science, vol.7, no.2, pp.57–76, 2013.
[4] C. Boyer and S. Roy, "Backscatter communication and RFID: Coding, energy, and MIMO analysis," IEEE Trans. Commun., vol.62, no.3, pp.770–785, 2014.
[5] K. Han and K. Huang, "Wirelessly powered backscatter communications networking: Modeling, coverage, and capacity," IEEE Trans.

Wireless Commun., vol.16, no.4, pp.2548–2561, 2017.
[6] V. Talla and J. Smith, "Hybrid analog-digital backscatter: A new approach for battery-free sensing," IEEE RFID, pp.74–81, 2013.
[7] J. Mitsugi, N. Rajoria, Y. Kawakita, and H. Ichikawa, "Wireless and batteryless vibration testing of space structures with implanted LSI sensors," 68th International Astronautical Congress (IAC), IAC-17, C2, X39637, 2017.
[8] "ISO/IEC 18000-63, Information Technology — Radio frequency identification for item management —, Part 63 parameters for air interface communications at 860 MHz to 960 MHz type C," 2015.
[9] J. Mitsugi and Y. Kawakita, "Efficient frequency sharing of baseband and subcarrier coding UHF RFID systems," IEICE Trans. Commun., vol.E92-B, no.12, pp.3794–3802, Dec. 2009.
[10] D. Bharadia, K.R. Joshi, and S.M. Kotaru, "BackFi: High throughput WiFi backscatter," ACM SIGCOMM, pp.283–296, 2015.
[11] P. Zhang, M. Rostami, P. Hu, and D. Ganesan, "Enabling practical backscatter communication for on-body sensors," ACM SIGCOMM, pp.370–383, 2016.
[12] A.B. Noel, A. Abdaoui, T. Elfouly, M.H. Ahmed, A. Badawy, and M. Shehara, "Structural health monitoring using wireless sensor networks: A comprehensive survey," IEEE Commun. Surveys Tuts., vol.19, no.3, pp.1403–1423, 2017.
[13] X. Fu, A. Pedross-Engel, D. Arnitz, C.M. Watts, and M.S. Reynolds, "Simultaneous imaging, sensor tag localization, and backscatter uplink via synthetic aperture radar," IEEE Trans. Microw. Theory Techn., vol.66, no.3, pp.1570–1578, 2018.
[14] R.Z. Doany, C. Lovejoy, K. Jones, and H. Stern, "A CDMA-based RFID inventory system: A CDMA approach as a solution for decreased power consumption," IEEE International Conference on RFID, pp.1–4, 2016.
[15] E. Vahedi, R.K. Ward, and I. Blake, "Performance analysis of RFID protocols: CDMA versus the standard EPC Gen-2," IEEE Trans. Autom. Sci. Eng., vol.11, no.4, pp.1250–1261, 2014.
[16] P. Hu, P. Zhang, and D. Ganesan, "Laissez-Faire: Fully asymmetric backscatter communication," ACM SIGCOMM, pp.255–267, 2015.
[17] G. Vannuci, A. Bletsas, and D. Leigh, "A software-defined radio system for backscatter sensor networks," IEEE Trans. Wireless Commun., vol.7, no.6, pp.2170–2179, 2008.
[18] K.A.S. Immink, Codes for Mass Data Storage Systems, Chap 8 DC-balanced Codes, Shannon Foundation Publishers, 2004.
[19] M. Varner, R. Bhattacharjea, and G.D. Durgin, "Realizing ReMoRa (reflection of modulated radio) ambient scatter communication links with perfect pulses," IEEE J. Radio Freq. Identif., vol.1, no.1, pp.59–67, 2017.
[20] B.P. Degnan and G.D. Durgin, "Aynchronous trigger modulation for RFID systems," IEEE Conference on RFID Technology and Applications, pp.153–158, 2015.
[21] Y. Igarashi, Y. Sato, Y. Kawakita, J. Mitsugi, and H. Ichikawa, "Feasibility study on simultaneous data collection from multiple sensor RF tags with multiple subcarriers," IEEE RFID, 2014.
[22] N. Rajoria, Y. Igarashi, J. Mitsugi, Y. Kawakita, and H. Ichikawa, "Concurrent backscatter streaming from batteryless and wireless sensor tags with multiple subcarrier multiple access," IEICE Trans. Commun., vol.E100-B, no.12, pp.2121–2128, Dec. 2017.
[23] J. Mitsugi, Y. Kawakita, K. Egawa, and H. Ichikawa, "Perfectly synchronized streaming from digitally modulated multiple backscatter sensor tags," IEEE Conference on RFID Technology and Application (RFID-TA), 2018.
[24] H. Chenling and H. Min, "New method of synchronization for RFID digital receivers," IEEE Solid-State and Integrated Circuit Technology, pp.1595–1597, 2016.

Jin Mitsugi received the B.S. from Nagoya University in 1985, M.S. and Ph.D. from Tokyo University in 1987 and 1996, respectively. He had been with NTT laboratory since 1987 pursuing a research and development on satellite communication system. He has been with Keio University since 2004. His research interests are network RFID, sensor network system, satellite communications and operations research

Yuki Sato received B.A., M.A. and Ph.D. from Keio University in 2012, 2013 and 2017, respectively. He is currently a project research associate in Graduate School on Media and Governance, Keio University. His research interests are RFID, unique identification technologies and their information systems, Internet of Things and wireless communications.

Yuusuke Kawakita received B.A., M.A. degree and Ph.D. from Keio University in 2000, 2002 and 2008, respectively. He is an associate professor at Kanagawa Institute of Technology. His present research interests focus on the ubiquitous sensing and its platform architecture.

Haruhisa Ichikawa received B.S., M.S., and Dr.Eng. degrees in electrical engineering from the University of Tokyo in 1974, 1975 and 1989, respectively. He joined NTT Laboratories in 1976, where he was engaged in fundamental research on communications software and distributed computing. He created and conducted many R&D projects for software, Internet, information sharing platform and ubiquitous networks, including business incubation. He was Executive Director of NTT Science and Core Technology Laboratory Group till 2007. He joined the University of Electro-Communications in 2007 and is a professor emeritus.